Journal of Catalysis 404 (2021) 594–606

Contents lists available at ScienceDirect

Journal of Catalysis

journal homepage: www.elsevier.com/locate/jcat

Acidity effect on benzene methylation kinetics over substituted H-MeAlPO-5 catalysts

Magnus Mortén [a], Tomás Cordero-Lanzac [a,b], Pieter Cnudde [c], Evgeniy A. Redekop [a], Stian Svelle [a], Veronique van Speybroeck [c], Unni Olsbye [a,*]

[a] Centre for Materials Science and Nanotechnology (SMN), Department of Chemistry, University of Oslo, N-0315 Oslo, Norway
[b] Department of Chemical Engineering, University of the Basque Country (UPV/EHU), PO Box 644, 48080 Bilbao, Spain
[c] Center for Molecular Modeling, Ghent University, Technologiepark 46, B-9052 Zwijnaarde, Belgium

ARTICLE INFO

Article history:
Received 14 September 2021
Revised 1 November 2021
Accepted 3 November 2021
Available online 12 November 2021

Keywords:
MTH
MTG
MTO
Computational
Experimental
Kinetics
Acid strength
AlPO-5
MeAlPO-5

ABSTRACT

Methylation of aromatic compounds is a key reaction step in various industrial processes such as the aromatic cycle of methanol-to-hydrocarbons chemistry. The study of isolated methylation reactions and of the influence of catalyst acidity on their kinetics is a challenging task. Herein, we have studied unidirectional metal-substituted H-MeAlPO-5 materials to evaluate the effect of acid strength on the kinetics of benzene methylation with DME. First-principle simulations showed a direct correlation between the methylation barrier and acid site strength, which depends on the metal substituent. Three H-MeAlPO-5 catalysts with high (Me = Mg), moderate (Me = Si) and low acidity (Me = Zr) were experimentally tested, confirming a linear relationship between the methylation activation energy and acid strength. The effects of temperature and reactant partial pressure were evaluated, showing significant differences in the byproduct distribution between H-MgAlPO-5 and H-SAPO-5. Comparison with propene methylation suggested that the Mg substituted catalyst is also the most active for the selective methylation of alkenes.

1. Introduction

Zeolite-catalyzed methylation of aromatic compounds to form e.g. toluene, xylenes and 2,6-dimethylnaphthalene is an important part of large scale petrochemical processes [1,2]. It is also a key step in the increasingly important Methanol-to-Hydrocarbons (MTH) process, an attractive route for the production of fuels and platform chemicals, starting from carbon-containing sources such as CO_2 and H_2, syngas, natural gas or biomass [3]. Especially, the Methanol-to-Olefins (MTO) and methanol-to-gasoline (MTG) processes have been widely studied in recent years [4–6], and several commercial plants are in operation [7]. There is now general consensus that the main autocatalytic species in the MTH conversion are alkenes and arenes that are confined in the micro-pores and cavities of the zeolitic catalyst [8]. Although a multitude of reactions may proceed over the Brønsted acid sites of the catalyst, methylation of alkenes and (polymethyl-)benzenes by methanol or dimethyl ether (DME) reactants, followed by cracking and dealkylation, respectively, to form C_2-C_4 alkenes, have been identified as main propagation reactions of the autocatalytic mechanism. This mechanism is often referred to as the Hydrocarbon Pool [9], or Dual Cycle mechanism [10], consisting of alkene and arene cycles that are interlinked by several reactions. The already mentioned dealkylation reactions is one such reaction class, by which a polymethylbenzene is converted to a light alkene and a lighter polymethylbenzene analogue [11]. Another example is hydrogen transfer reactions, where methanol acts as a hydrogen-transfer mediator for conversion of light alkenes to the corresponding alkane and a methylated diene. Further coupling and hydrogen transfer reactions subsequently lead to formation of the aromatic compounds [12]. Methanol- or DME- induced hydrogen transfer reactions are also central to the formation of the first C-C bond from the oxygenate feed [4,13], and to the conversion of polymethylbenzene into polycyclic aromatics and, eventually, coke [14].

Prior studies of methylation reactions involved in the MTH process showed that they take place over the Brønsted acid sites following either a concerted or stepwise pathway [14–16]. According to the concerted mechanism, methanol or DME reacts directly with the co-adsorbed hydrocarbon, thereby producing a methylated product and releasing a water or methanol molecule,

* Corresponding author.
E-mail address: unni.olsbye@kjemi.uio.no (U. Olsbye).

https://doi.org/10.1016/j.jcat.2021.11.002
0021-9517/

respectively. In the stepwise mechanism, on the other hand, a surface methoxy species (SMS, CH_3-Z) is first formed from one of the oxygenates. In turn, SMS reacts with the hydrocarbon, producing the final methylated compound. Therefore, the abundance of SMS and the relative reactivity of hydrocarbons towards SMS vs. adsorbed oxygenates determine the nature of the dominant methylation mechanism under specific conditions.

Saepurahman et al. [17] performed *in-situ* FT-IR experiments of benzene methylation over H-ZSM-5 and H-beta zeolites at 250–400 °C, where the absence of SMS on Brønsted acid sites was suggested. However, the contribution of the stepwise mechanism was not discarded due to the low concentration of intermediates during efficient reaction conditions. Hill et al. [18] studied the methylation of benzene, toluene and xylenes over a H-ZSM-5 zeolite using very low reactant partial pressures. They observed a shift between the predominant surface species from SMS (for benzene and toluene reactions) to co-adsorbed xylenes and SMS. According to the theoretical results reported by Deluca et al. [16], benzene methylation should predominantly occur through the stepwise mechanism at reasonable temperature and pressure conditions (80–350 °C and 0.2–1 bar), with the formation of SMS being the rate-limiting step and energetically favored in the presence of a neighboring adsorbed arene. Otherwise, a shift of the dominating mechanism from concerted to stepwise was proposed by Wen et al. [19] to occur at 400 °C over H-ZSM-5 and H-beta zeolites. The methylating agent also influences the reaction rate and in this sense, higher rates for benzene and toluene methylation are reported when DME is used instead of methanol at the same reaction conditions [14,20]. Overall, the extent and rate of methylation reactions are primarily affected by the reaction conditions, the density and strength of acid sites and the topology of the host framework.

H-SAPO-34 and H-ZSM-5 are the most studied catalysts for the MTH reactions due to their selective production of olefins and gasoline-type hydrocarbons, respectively [21]. The CHA structure of H-SAPO-34 presents big cavities interconnected by small 8-ring windows, resulting in a severe shape selectivity. The polymethylbenzene (PMB) intermediates can be easily methylated within the zeotype cavities in a mechanism dominated by the arene cycle [22]. However, the hindered diffusion of these molecules direct the reaction towards a selective formation of light olefins and a fast deactivation [23–25]. Recently, it was also shown that the presence of Brønsted acid sites on the catalyst has a promotional effect on the diffusion of light olefins [26,27]. On the contrary, the 3-dimensional MFI structure of H-ZSM-5, with intersecting zig-zag and straight 10-ring channels, favors the evolution of secondary reactions and therefore the formation of aromatics and long-chained hydrocarbons [28]. Particularly in this case, the acid strength of the zeolite has a strong influence on the product distribution [29,30].

Other aluminophosphates, such as AlPO-5 with the AFI topology, formed by large one-dimensional 12-ring channels of 7.3 Å diameter, allow for a faster diffusion of reaction products and, therefore, limit secondary reactions [31]. The isomorphous substitution of the Al or P atoms in these materials by Me^{2+} or Me^{4+} species, respectively, were reported to provide structures with stable Brønsted acid sites using heteroatoms as Si, Co, Zn, Zr or Mg [31–36]. H-SAPO-5 is especially interesting because it presents a similar acidity to those of the commercial H-SAPO-34 catalysts for the MTO process and because its channels have a similar size as the cavities of H-SAPO-34 [37]. Moreover, its open structure, without the small windows of CHA structure, makes it a suitable option for monitoring the first stages of the methylation reaction by co-feed control experiments. According to theoretical calculations of Zhang et al. [38], the topology of the H-SAPO-5 promotes the alkene cycle during the MTO reaction. Furthermore, several experimental observations have highlighted that the product distribution can be modulated by using isomorphically substituted H-MeAlPO-5 catalyst [31,39].

Recent computational studies suggested a linear relationship between acid strength and the activation energy of alkene methylation reactions in H-MeAlPO materials with CHA, AEI and AFI topology [40–42]. This correlation has yet to be experimentally verified. In prior contributions, we explored the effect of acid strength between H-SAPO-5 and its zeolite analogue, H-SSZ-24, for benzene and propene methylation reactions in the context of the MTH conversion [43,44]. Using methanol as the methylating agent, those contributions showed that the abundance of competing reactions was so high that it was not possible to deduce kinetic parameters for the methylation reactions [44]. Based on the results obtained, a reaction scheme illustrating the different pathways from benzene and methanol over Brønsted-acidic catalysts was presented. An updated version of the scheme is shown as Fig. 1 below. Later, we learned that methanol is a prominent hydrogen transfer agent, and that DME yields fewer byproducts than methanol when used as a methylating agent over H-ZSM-5 [14].

Armed with this insight, the aim of the present study is to explore the influence of acid strength on benzene methylation kinetics with DME as methylating agent over a series of H-MeAlPO-5 materials, by performing a combination of first-principle simulations and experimental measurements. The material series covers high, medium and low acid strength, i.e.; Me = Mg, Zn, Co, Si, Ti and Zr. DFT calculations allow us to explore the influence of the acid strength on the co-adsorption behavior of DME and benzene as well as on the intrinsic methylation barriers. Through kinetic experiments, the effect of the reaction conditions has been evaluated, and the contrasting acid strength of the samples have allowed a comparison between the methylation reaction rate, apparent activation energy and product distribution for each catalyst. Finally, methylation rates of benzene and propene over the H-MgAlPO-5 and H-SAPO-5 catalysts were compared at 400 °C.

2. Materials and methods

2.1. Computational methodology

To investigate the correlation between the acidity of MeAlPO-5 zeotype frameworks and the adsorption and methylation characteristics of benzene with DME, a combination of static DFT calculations and molecular dynamics (MD) simulations were performed. Static DFT calculations were performed to quantify the adsorption strength of DME and benzene as well as the barrier for concerted benzene methylation. By carrying out MD simulations, the conformational freedom and mobility of the (co-)adsorption of DME and benzene were analyzed.

First-principle simulations were performed on a periodically extended $1 \times 1 \times 2$ supercell of the AFI framework, containing 48 T atoms. The AFI lattice consists of straight 12-ring sized channels. A single Brønsted acid site per unit cell was considered, corresponding to a (Al + P)/Me ratio of 47. The Brønsted acid sites in the MeAlPO-5 zeotypes were generated by isomorphic substitution of either a P atom by a Si, Ti or Zr atom (oxidation state + 4) or an Al atom by a Mg, Co or Zn atom (oxidation state + 2) and adding a charge-compensating proton at the O2 position, thus resulting in a series of isostructural materials with varying acid site strength. Depending on the nature of the doping element, materials with high acidity (Mg, Co, Zn), medium acidity (Si) or low acidity (Ti, Zr) were obtained. For comparison, also the aluminosilicate version of the AFI topology, H-SSZ-24 is included in our study.

Static periodic DFT calculations were carried out using the Vienna Ab Initio Simulation Package (VASP 5.4) [45–48] to deter-

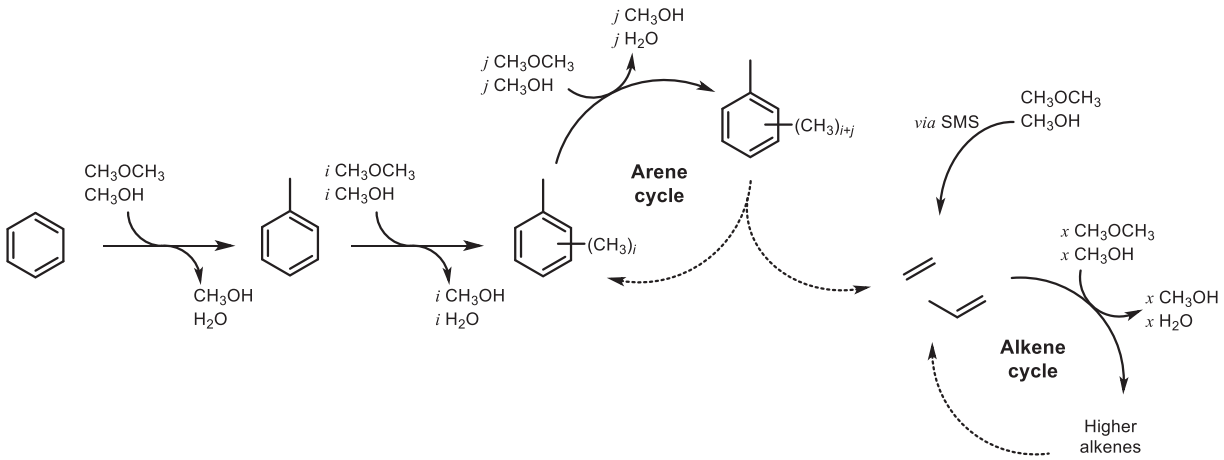

Fig. 1. Expected reactions and products (excluding coke) during co-feed of benzene and DME/MeOH according to the dual-cycle mechanism. . Adapted from [14]

mine the adsorption strength of ammonia, DME and benzene as well as the intrinsic barrier for benzene methylation in the series of H-MeAlPO-5 materials. As level of theory, the PBE functional with additional Grimme D3 dispersion corrections was chosen [49,50]. The Projector Augmented Wave (PAW) method was applied together with a kinetic energy cutoff of 600 eV for the plane wave basis set [51–53]. The sampling of the Brillouin zone is restricted to the Γ-point. For the local minima, all structures were relaxed using a conjugate gradient method with an electronic convergence criterion of 10^{-5} eV and an ionic relaxation threshold of 10^{-4} eV. Transition states were initially localized with the improved dimer method [54], and then refined with a quasi-Newton algorithm as implemented in VASP. The reactant and product states were found by following the intrinsic reaction coordinate from the transition state, i.e., displacing the geometry along the normal mode corresponding to the methylation reaction. The nature of the stationary states was verified by a normal mode analysis (NMA). The vibrational modes were determined from a partial Hessian vibrational analysis (PHVA) including an 8 T cluster of the zeolite framework around the acid site and the adsorbed hydrocarbons [55–57]. Thermal corrections at finite temperature were derived based on the harmonic oscillator approximation using the TAMkin software package [58]. The optimal cell volume and corresponding cell parameters were determined for the empty H-SAPO-5 unit cell by a least square fit to the Birch-Murnaghan energy vs. volume equation of state [59]. The resulting cell parameters (a = 13.92 Å, b = 13.96 Å, c = 17.03 Å, α = 90.05°, β = 90.03° and γ = 119.49°) and volume (2879.64 $Å^3$) were kept fixed during all geometry relaxations. Analogously, for H-SSZ-24, the cell parameters (a = 13.86 Å, b = 13.82 Å, c = 16.84 Å, α = 90.03°, β = 89.97° and γ = 120.69°) and volume (2773.93 $Å^3$) were also kept constant.

Ab initio molecular dynamics simulations on a fully periodic unit cell of the metal substituted AlPO-5 materials in which DME (and benzene) are adsorbed were carried out at the revPBE-D3 level of theory [49,50,60], with the CP2K software package (CP2K3.0) [61,62]. The Gaussian and plane wave (GPW) basis set approach [63,64] was adopted with an energy cutoff of 320 Ry for the plane wave basis. A localized double zeta valence polarized basis set and GTH pseudopotentials were used (DZVP-GTH) [65–67]. The sampling of the free energy surface in the MD simulations occurs in the NpT ensemble at 350 °C and 1 atm, in which the zeolite framework is fully flexible. The temperature is controlled by a chain of 5 Nosé-Hoover thermostats [68,69] and the pressure by an MTK barostat [70]. After an equilibration run of 5 ps, a production run of 80 ps with an integration time step of 0.5 fs was carried out. A selection of snapshots from the MD simulations was used as input for static geometry optimizations on the relevant adsorption complexes. A geometrical analysis of the sampled configurations employing different criteria was carried out to select the most probable conformations of the guest molecules.

2.2. Experimental procedures

2.2.1. Catalyst materials

Methylation reaction was analyzed over three H-MeAlPO-5 catalysts (Me = Mg, Si, or Zr) with the same AFI topology, but different acidity. The inclusion of these heteroatoms in the AFI structure substantially modifies the acidity of the samples. The synthesis procedure of each catalyst can be found elsewhere [31]. The main physico-chemical properties of the used catalysts are summarized in Table 1. As shown in the table, all samples exhibit similar specific surface area (S_{BET}), while the main differences are found in acid site density, from n-propylamine adsorption-TPD experiments, and estimated desorption heat of the base probe molecule (NH_3), from computational calculations. Due to the complex interaction of NH_3 with AlPO-5 and SAPO-5 [71], no attempt was made to experimentally measure NH_3 adsorption heats.

2.2.2. Catalytic tests

Catalytic tests were carried out in a fixed bed quartz reactor of 8 mm diameter at atmospheric pressure. The catalyst was sieved to a particle size of 250–420 μm and mixed with calcined and sieved quartz particles to obtain the same weight of catalyst plus inert in each experiment. Reaction temperature was monitored by a thermocouple protected by a 3 mm wide quartz sleeve inserted into the middle of the catalytic bed. Prior to the reactions, the catalysts were activated at 550 °C. The temperature was raised up at 5 °C min^{-1} under 20% O_2 in N_2 flow. Then, the gas flow was switched to pure oxygen, and the activation temperature was maintained isothermal for 1 h. The temperature was then cooled down to the reaction temperature at 5 °C min^{-1}.

Methylation reactions were performed by co-feeding benzene (Sigma-Aldrich Chroma Solv, 99.9%) and dimethyl ether (DME, Praxair or AGA, 25 %DME/argon 6.0) as reactants. Benzene was fed by bubbling a continuous stream of He into a flask of boiling reactant. The saturated He stream was then passed upwards through a water-cooled Vigreux condenser at 35 °C by a circulating thermostat water bath. The catalysts were tested in different sets of experiments. Each set consisted of reaction-regeneration cycles to ensure full activity of the catalyst in each single run. The procedure followed for the regeneration was the same above explained for the catalyst activation. Moreover, the central experimental

Table 1
Physico-chemical properties of the H-MeAlPO-5 catalysts.

Catalyst	Crystal Size (μm)	S_{BET} ($m^2\ g^{-1}$)	Acid site density (mmol g^{-1})[a]	Density of Me (mmol g^{-1})[b]	ΔE_{NH3} (kJ mol^{-1})[c]
H-MgAlPO-5	1 × 2.5	360	0.102	0.1	−170
H-SAPO-5[c]	1 × 2	340	0.085	0.3	−135
H-ZrAlPO-5	2 × 4.5	352	0.065	-[d]	−117

[a] Determined by n-propylamine TPD.
[b] Estimated from EDS, based on ratio of Me and either Al or P.
[c] Computed from ammonia adsorption simulations.
[d] Overlap between Zr/P peaks, no estimate obtained.

point was sequentially repeated in order to obtain consistent results, thus monitoring potential irreversible deactivation of the materials. Within each of these sets of reactions, results were internally consistent but some deviations were observed in the absolute conversion values from set to set, which could be ascribed to analysis errors at the very low conversion levels studied, slightly different on-set conditions or different storage time of the samples. In any case, these small discrepancies do not affect the trends neither within each set of experiment nor among the different sets.

To evaluate the activity of the catalysts, the effect of temperature was tested first. These experiments were carried out using a fixed amount of each catalyst in the reaction temperature range of 250–450 °C. Fixed partial pressures of benzene (80 mbar) and DME (20 mbar) were used. The influence of each reactant on methylation was evaluated by performing a second set of experiments using the H-MgAlPO-5 and H-SAPO-5 catalysts, where the partial pressure of each reactant was varied in the temperature range of 300–400 °C. In one series of experiments, DME partial pressure was fixed to 40 mbar and benzene partial pressure was varied from 20 to 100 mbar. In another series, benzene partial pressure was likewise fixed to 40 mbar and that of DME was varied from 20 to 100 mbar. In all these tests of temperature and partial pressure variation, the gas hourly space velocity (GHSV) was constant for each used catalyst and reaction conditions.

Experiments at different contact time (space time, g s cm^{-3}) were also carried out, using the H-MgAlPO-5 and H-SAPO-5 catalysts at 400 °C to estimate the initial benzene methylation rate. The contact time was modified by simultaneously adjusting the flow rates of the reactants and pure helium, using values up to 86 and 115 g s cm^{-3} for the H-MgAlPO-5 and H-SAPO-5 catalysts, respectively. The methylation of benzene, a primary reaction of the aromatic cycle of the dual-cycle mechanism, was compared with the methylation of propene, which can be considered as the analogue primary reaction of the alkene cycle. Propene (AGA 5.0) methylation reactions were carried out at the same conditions. However, slightly higher values of contact time were required, using a maximum of 144 g s cm^{-3} for both catalysts. Moreover, the individual partial pressure of each reactant was different due to the nature of the reactions. The main byproducts in benzene methylation are polymethylbenzenes, while propene methylation competes mainly with oligomerization (and cracking) reactions, competing reactions involved in the dual-cycle mechanism.

The effluent from the reactor was analyzed after 5 min of reaction (10 min for propene methylation), by an on-line GC–MS instrument (Agilent 7890, with a flame ionization detector, and Agilent 5975C, with a MS detector) by using two Restek Rtx-DHA-150 columns, and hydrogen (Praxair, purity 6.0) as the carrier gas. Individual conversions of benzene (B) and oxygenates (dimethyl ether, DME, and methanol) were defined as

$$X_{benzene}(\%) = \frac{F_{rings}}{F^0_{Benzene}} 100 \quad (1)$$

$$X_{OX}(\%) = \frac{F_{CH_3}}{F^0_{DME}} 100 \quad (2)$$

where $F^0_{Benzene}$ is the flow rate of benzene molecules and F^0_{DME} is the flow rate DME in contained C units at the inlet of the reactor, respectively. Under the assumption that all benzene rings in aromatic molecules originate from benzene, while all methyl groups in those aromatic molecules, as well as all aliphatic products, originate from DME: F_{rings} is the flow rate of aromatic ring-containing product molecules at the outlet of the reactor, and F_{CH3} is the flow rate of aliphatic products and branches anchored to aromatic rings in contained C units at the outlet of the reactor.

3. Results and discussion

3.1. Computational characterization of benzene methylation

Insight into the influence of acid strength on the rates of key elementary reactions is an essential element for the *in silico* catalyst design and can be achieved by studying isomorphous metal substituted zeotypes or zeolites. Herein, we examine the reactivity for benzene methylation on a series of metal substituted AlPO-5 materials, which all exhibit the same AFI framework topology, differing solely in the nature of the substituted metals and hence in the Brønsted acid strength. The ammonia adsorption energy was successfully proposed as a descriptor for the acidity of the active sites for this set of materials [31,40,41,72–74], with H-MgAlPO-5 showing the strongest and H-ZrAlPO-5 showing the weakest acid sites. This trend is confirmed by the nature of adsorbed ammonia in the different frameworks, i.e., in the most acidic H-MgAlPO-5, H-ZnAlPO-5, H-CoAlPO-5 and H-SAPO-5 materials, ammonia exists in a stable protonated state, NH_4^+, forming H-bonds with the framework, while in the weaker acid materials H-ZrAlPO-5 and H-TiAlPO-5 neutral ammonia is adsorbed at the acid sites. Values of the ammonia adsorption energy calculated for the H-MgAlPO-5, H-SAPO-5 and H-ZrAlPO-5 are shown in Table 1. Given the same topology of all considered AlPO framworks – varying only in the nature of the substituted metal, it can be safely assumed that the entropy contributions will be similar in all materials and that any variation in the adsorption or methylation activity is fully captured by the (de)stabilizing enthalpic interactions. Furthermore, accurately estimating finite temperature effects and thermal corrections is far from trivial in static DFT calculations [75–78]. Therefore, electronic energies are reported hereafter, while for completeness, the adsorption thermodynamics and methylation barriers at 350 °C can be found in Section S1 of the Supplementary Material.

The methylation of benzene with DME can either occur through a concerted or stepwise mechanism. Note that the preferred pathway might change depending on the reaction conditions, catalyst acidity and framework topology [16–20]. Experimentally, it is challenging to distinguish the governing methylation mechanism and it is likely both pathways are operational in most practical cases.

Some theoretical studies addressed the competition between the mechanisms and noted that the stepwise methylation may be prevalent at higher temperatures or lower pressures [79–81]. At the moderate experimental conditions used in this work and, moreover, at industrially-relevant conditions of elevated reactant partial pressures, the concerted methylation reaction is expected to play a major role and hence is the focus of the computational part.

The reaction energy diagram for adsorption and methylation of benzene with DME in the H-MeAlPO-5 materials, obtained using static DFT calculations, is displayed in Fig. 2. The results clearly reflect the acidity trend with the strongest adsorption of DME, co-adsorption of benzene and lowest methylation barrier in the highly acidic H-MgAlPO-5 (and to a somewhat lesser extent H-ZnAlPO-5 and H-CoAlPO-5) material. The lowest adsorption strength and corresponding high methylation activation energies are found for the least acidic H-ZrAlPO-5 and H-TiAlPO-5 frameworks while H-SAPO-5 is located in between. As expected, the co-adsorption of DME and benzene bind more tightly to the strongest acidic sites. The activation energy for methylation also decreases for higher acid site strengths, which might be understood by an enhanced proton transfer ability and stabilization of ion-like intermediates and transition states in the more acidic materials [41,44,82].

A major shortcoming of the static approach is that only a limited number of states on the potential energy surface, often a single local minimum for each intermediate, are taken into account. However, the potential energy surface for adsorption of hydrocarbons in porous zeolites is typically quite complex, exhibiting various, often quasi-isoenergetic stationary states [44,83–86]. Therefore, first-principle MD simulations at 350 °C were performed to explore the configurational freedom of the adsorbed DME and co-adsorbed benzene species and validate whether the states found so far were representative at true reaction conditions. A geometrical analysis of the most sampled configurations can reveal valuable insight into the behavior of the adsorption complexes (see Section S2 of the Supplementary Material). Subsequently, a geometry optimization on these identified configurations was carried out to assess the energy spread on the different adsorbate orientations and to ensure that (one of) the most stable configurations of the adsorption complexes has been localized. Our results reveal that none of the other frequently sampled configuration results in a more stable configuration upon relaxation and that therefore the current approach for determining the pre-reactive adsorption complexes by following the reaction coordinate adequately determines the preferred adsorbate geometries for this specific case of DME and benzene co-adsorption.

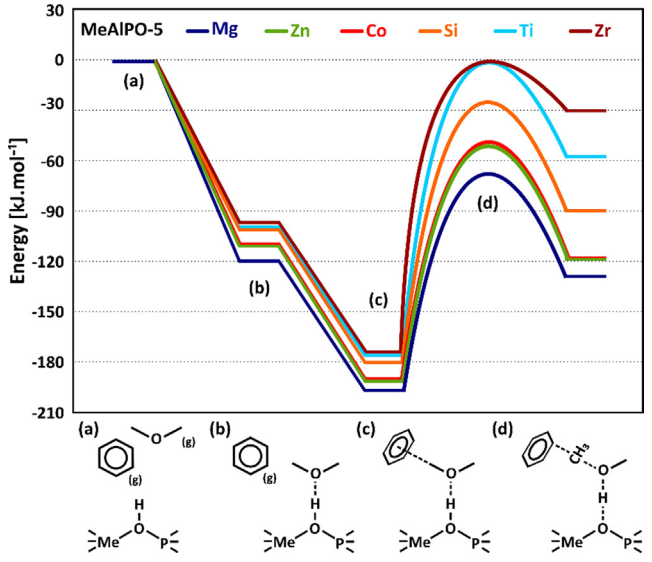

Fig. 2. Reaction electronic energy diagram for the adsorption of DME, co-adsorption of DME and benzene and concerted methylation reaction of benzene with DME at the acid sites of the metal substituted H-MeAlPO-5 materials (Me = Mg, Zn, Co, Si, Ti or Zr) with reference to benzene and DME in gas phase and the empty framework. LOT: PBE-D3.

Fig. 3**a** shows the correlation between the intrinsic energy barriers for the concerted benzene methylation with DME and the acid strength, quantified by the ammonia adsorption energies for the H-MeAlPO-5 materials. In addition, the correlations between this acid strength and DME adsorption energy, DME and benzene co-adsorption energy and the resulting values of the apparent energy barriers for methylation are shown in Fig. 3**b and 3c**, respectively. The calculations clearly demonstrate the existence of a linear trend in all cases, with the lowest benzene methylation barriers and adsorption energies observed for the most acid frameworks. Analogously to the previously demonstrated linear scaling relations for the methylation of small olefins (with methanol) as exemplary reactions for the alkene cycle in the MTH process [40–42], the current results point to a similar linear relation for the methylation reactions (with DME) occurring in the arene cycle. Chen et al. [87] also reported a linear relationship between the methylation free energy barrier and pyridine adsorption free energies for different catalysts, thus indicating that the adsorption energy of the probe molecule can be used as a reliable descriptor to predict methylation energy barriers.

The slope of the linear fit represents the sensitivity of the reaction energy barrier to the acid site strength and is critically determined by the framework ability to enthalpically stabilize the involved transition states or intermediates. Transformations involving transition states that exhibit high ion-pair like characteristics such as the concerted methylation reactions are therefore expected to have a higher sensitivity for the acid strength [41]. The theoretical slope for concerted benzene methylation (0.83, Fig. 3**a**) is somewhat lower than the slopes for concerted small alkene methylation (1.06–1.09) reported by Studt and coworkers [42]. This observation may be attributed to the higher stability of the ion-like transition state for benzene methylation compared to ethene/propene methylation due to the presence of the aromatic π-electron system, evidently resulting in a lower sensitivity to the acid site strength. However, some caution is warranted in quantitatively comparing the slopes of the two theoretical approaches, as the current results are obtained with a different level of theory, which may also induce significant variations in the slope of the linear relation.

Albeit having a distinctly different framework composition, it can be noticed that the aluminosilicate zeolite H-SSZ-24 is also quite well described by the scaling trend for the MeAlPO-5 materials, thus also corroborating the findings by Studt and coworkers for alkene methylation [40–42]. When comparing the reactivity of H-SAPO-5 with the more acidic H-SSZ-24 for methylation reactions, it was previously shown that the geometric configuration of the pre-reactive co-adsorption complex, formed upon methylation, may be distinctly different for the aluminophosphate and the zeolite material [44]. Likewise, benzene methylation with methanol was reported to be relatively more preferred on the more acidic framework, which is in agreement with the hypothesis that the slope for benzene methylation is lower than for alkene methylation [44].

Following the same trend as the intrinsic methylation barriers, the highest DME (and benzene) adsorption strength is found for the most acidic materials (Fig. 3**b**). Both the adsorption energies and the intrinsic methylation barriers are clearly sensitive to the acid strength, although the sensitivity is much more pronounced for the intrinsic methylation energy barrier than for the reactant

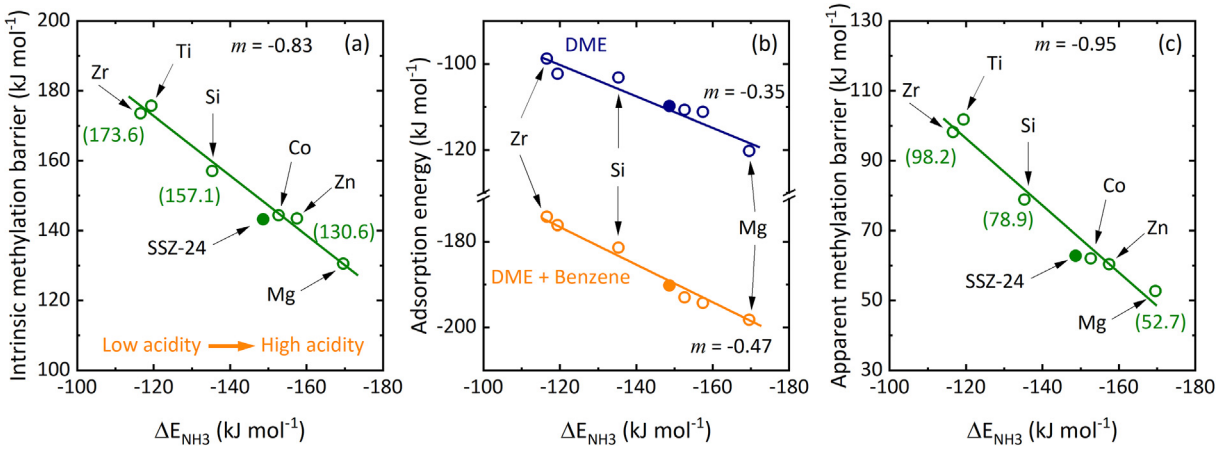

Fig. 3. Linear scaling relation between the ammonia adsorption energies and the (a) intrinsic electronic energy barriers for concerted benzene methylation with DME, (b) DME adsorption and DME and benzene co-adsorption electronic energies and (c) apparent energy barriers for concerted benzene methylation with DME on the metal substituted H-MeAlPO-5 catalysts (Me = Mg, Zn, Co, Si, Ti or Zr) and H-SSZ-24. LOT:PBE-D3 (m is the slope of the linear trend $y = mx + b$).

(s) adsorption due to the high ionic character of the benzene methylation transition state. This observation is evidenced by the lower slope values of 0.35 or 0.47 for the linear trend of respectively DME adsorption and co-adsorption of DME and benzene on the acid sites, (Fig. 3**b**) compared to a slope of 0.83 for the methylation barrier (Fig. 3**a**). Note that the co-adsorption of benzene is more sensitive to the acid strength than the adsorption of DME despite the fact that benzene is not directly adsorbed on the acid site but rather near the methyl groups of DME. The largest impact of the acid strength is therefore found on the intrinsic reactivity of benzene methylation while there is also a smaller, but non-negligible impact on the DME (and benzene) adsorption. As a result, the impact of the acid strength on the apparent methylation barrier will be higher than on the intrinsic methylation barrier, as confirmed by the higher slope value (0.95, Fig. 3**c**).

3.2. Catalytic testing of substituted H-MeAlPO-5

Three characteristic H-MeAlPO-5 samples with high (H-MgAlPO-5), medium (H-SAPO-5), and low acidity (H-ZrAlPO-5) were selected for the experimental benzene methylation tests. Their main physico-chemical properties are shown in Table 1. Plots of benzene and oxygenates conversion versus temperature are depicted in Fig. 4**a-c,** and the corresponding formation rates of the main products are illustrated in Fig. 4**d-f.** As expected, both conversion and individual rates increase with temperature in all cases. Within the operational limits of the test rig, similar conversion levels were obtained over H-MgAlPO-5 and H-SAPO-5 by testing H-SAPO-5 at longer contact times, but H-ZrAlPO-5 gave substantially lower conversion at each temperature (Fig. 4**a-c**). Hence, direct selectivity comparisons may only be pursued for H-MgAlPO-5 and H-SAPO-5.

Reaction products can be grouped into three different families of compounds: toluene, polymethylbenzenes (PMB) and aliphatic products. The primary product, toluene, is the main product of reaction over all materials, followed by aliphatic products and polymethylated benzene (PMB), in the full temperature range (250–450 °C). Comparing the selectivity of H-SAPO-5 and H-MgAlPO-5, remarkable differences are observed between aliphatic and PMB trends. Without considering 250 °C due to the low conversion level, the ratio between the formation rates of toluene and byproducts is slightly higher for the H-SAPO-5 catalyst (**Fig. S8a**). Moreover, the formation rate of PMBs is faster with the H-MgAlPO-5 catalyst, whereas aliphatics are clearly the main byproducts of the reaction using the H-SAPO-5 catalyst (**Fig. S8b**), even competing with the formation rate of toluene at the highest temperature of 450 °C (192 and 129 mol $mol_{H+}^{-1}h^{-1}$, Fig. 4**e**). This result could suggest a promotion of the benzene methylation pathway by H-MgAlPO-5 and of alkene cycle-related competing reactions (vide infra) with H-SAPO-5. A similar trend has previously been observed when comparing the benzene methylation activity of H-SAPO-5 to its more acidic zeolite analogue, H-SSZ-24, using methanol as methylating agent [43].

Focusing next on the product distribution within the aliphatic and aromatic range, typical product distributions for benzene methylation over H-MeAlPO-5 catalysts at 400 °C are depicted in Fig. 5**a**. Considering first the aromatic products, they are dominated by polymethylated benzene molecules, which are byproducts originating from sequential methylation of benzene, toluene, xylenes and so forth, with the same reaction pathway. A decreasing abundance is expected with each stepwise methylation reaction, and this expectation is met by the experimental findings, with one exception: pentamethyl benzene is formed in surprisingly high amounts in both H-MgAlPO-5 and H-SAPO-5. For H-ZrAlPO-5, toluene and xylene were the only methylated benzene molecules observed, due to the very low conversion. Theoretical studies on PMB methylation with methanol or dimethyl ether have demonstrated that methylation barriers decrease with an increase in the number of methyl groups of the molecule [16,88,89]. However, the framework topology plays an important role in the product selectivity due to electrostatic interaction and steric hindrances. Deluca et al. [16] found minimum free energy values for tetraMBs within MFI framework, whereas Fecik et al. [89] reported an energy-favored state for pentaMB within the larger cavity of CHA framework. The open 12-ring AFI structure of the H-MeAlPO-5 series is expected to perform comparably to CHA because of the similar size of their cavities. This may explain the high concentration of pentaMB observed for the H-MgAlPO-5 and H-SAPO-5 catalysts (Fig. 5**a**). Indeed, our observation is consistent with the methylation barriers (115 and 169 kJ mol^{-1} for the methylation of tetraMB and pentaMB, respectively) reported by Fecik et al. [89] at 400 °C and 1 bar, conditions at which our experiments were carried out.

Aliphatic byproducts, formed through secondary and competing reactions (vide supra, Fig. 1), were observed in the product stream of all tests, but conversely to the PMB behavior, their selectivity varied with reaction temperature (**Fig. S9-S10**). Fig. 5**b** shows the carbon distribution of the aliphatic fraction obtained at 300 and 450 °C, over H-SAPO-5 and H-MgAlPO-5. Mostly C_4 and C_{5+} aliphat-

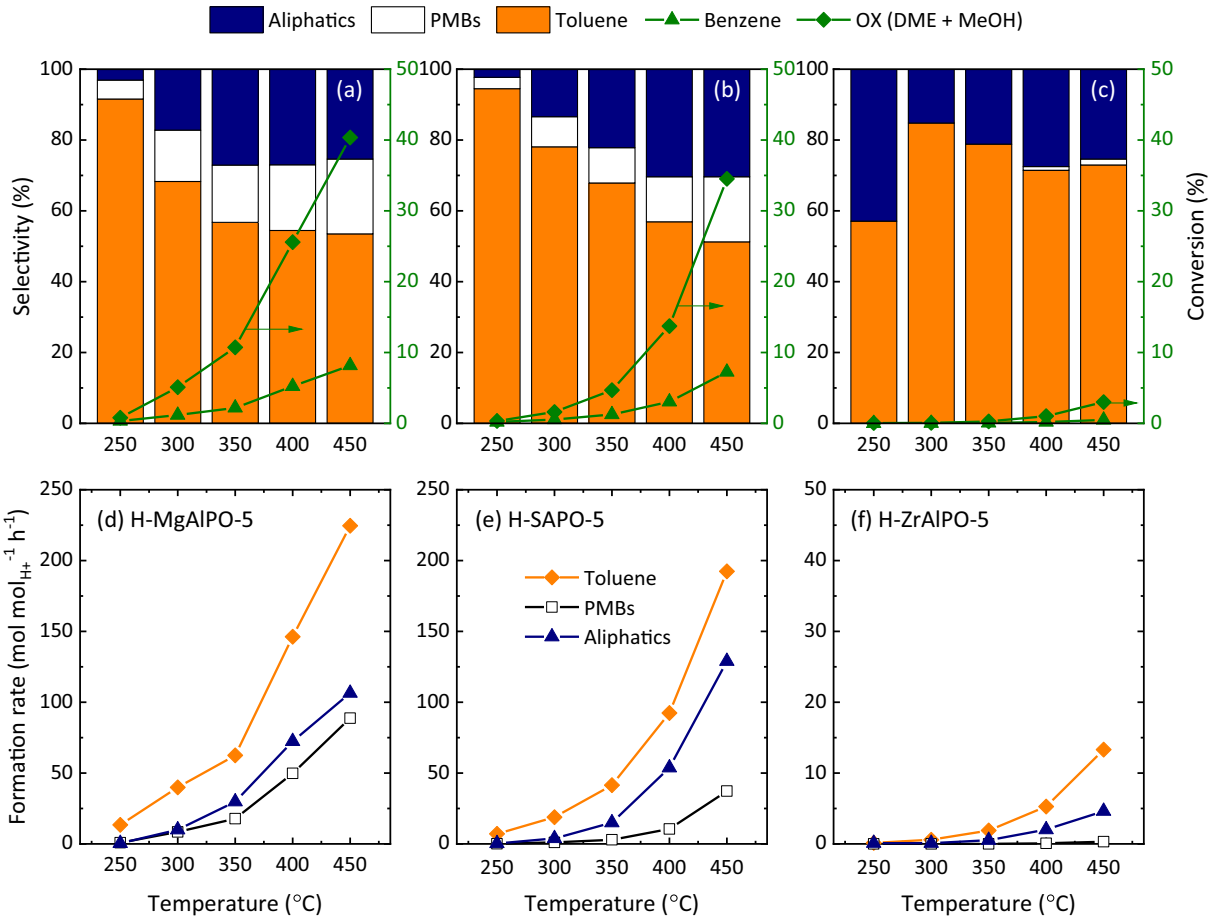

Fig. 4. Evolution with temperature of (a-c) the selectivity to the main reaction products, benzene and oxygenates conversions and of (d-f) the formation rates of the main reaction products for the (a) H-MgAlPO-5 (GHSV = 34 cm^3 g^{-1} s^{-1}), (b) H-SAPO-5 (GHSV = 26 cm^3 g^{-1} s^{-1}) and (c) H-ZrAlPO-5 catalysts (GHSV = 15 cm^3 g^{-1} s^{-1}). $P_{Benzene}$ = 80 mbar, P_{DME} = 20 mbar.

ics are observed at the lowest temperature, whereas the highest temperature leads to a maximum in the C_3 and C_4 aliphatics. The cracking of long hydrocarbons, a pertinent reaction of the alkene cycle of the dual-cycle mechanism (Fig. 1), is increasingly relevant at high temperatures, where the MTH reaction is fast [90]. The cracking of C_{5+} to C_3 aliphatics is also more remarkable over the H-MgAlPO-5 catalyst than over H-SAPO-5 with increasing temperature. This result is consistent with our previous work [31], where these materials were tested in the MTH reaction and alkene cracking was clearly promoted within H-MgAlPO-5 compared to H-SAPO-5. Also previously, acidity was reported as a driving factor to enhance and tune hydrocarbons cracking [91]. In particular, the large cavities of H-SAPO-5 catalyst were found to hinder 2-pentene monomolecular cracking pathway at 500 °C, and to promote oligomerization-cracking pathway instead [92]. Furthermore, the acidity of H-SAPO-5 was observed to be insufficient to produce significant amounts of C_3 during the oligomerization of ethene/butene [93].

The evolution of alkane distribution in the product stream with temperature is shown in Fig. 5**c**. Saturated products were not observed for the H-ZrAlPO-5 catalyst, possibly due to the very low conversion obtained with this catalyst. Indeed, significant concentrations of alkanes were only observed at 300 °C, when the most acidic H-MgAlPO-5 catalyst yielded an alkane to aliphatic ratio of 0.22. A higher yield of hydrogen transfer products (i.e. alkanes) at lower temperature was previously reported in the MTH reaction [94], and so was the promotion of hydrogen transfer reactions using catalysts with high acid site density [95] and acid strength [96]. Overall, a low contribution of the hydrogen transfer mechanism, a competing reaction in this catalytic system [12], can be deduced. Although it is not expected to play a big role due to the low benzene conversion levels (Fig. 4) and a zero-order dependency in benzene for aliphatics formation (vide infra), the dealkylation of PMBs should also be mentioned as a potential source of aliphatic compounds. This mechanism is usually reported as the main source of olefins in aromatic cycle-dominated MTH systems [11].

Considering next the temperature correlation of benzene methylation rates over each catalyst, the aforementioned trends in product distribution warrant the inclusion of all benzene methylation products when calculating benzene methylation rates (Fig. 6**a**). A linear trend is observed in all cases, with the rate values for H-MgAlPO-5 and H-SAPO-5 catalysts being significantly higher than those for the H-ZrAlPO-5 catalyst. All data fit the Arrhenius plot linearization with regression coefficients near unity. Apparent activation energy values, which were estimated from this linearization, present a linear correlation with the ammonia adsorption energies on Brønsted sites (Fig. 6**b**), a descriptor of acid strength, suitable for monitoring adsorption and intrinsic barriers in our particular reaction (**see** Fig. 3). In agreement with the computational results, H-MgAlPO-5 exhibits the lowest apparent activation energy value (44.6 kJ mol^{-1}), whereas H-ZrAlPO-5 catalyst shows the highest value (72.0 kJ mol^{-1}). Apparent activation barriers of ca. 58 kJ mol^{-1} were previously found for H-ZSM-5 and H-beta zeolites with similar Si/Al ratio, although their different topology led to different product distributions [17]. The activation

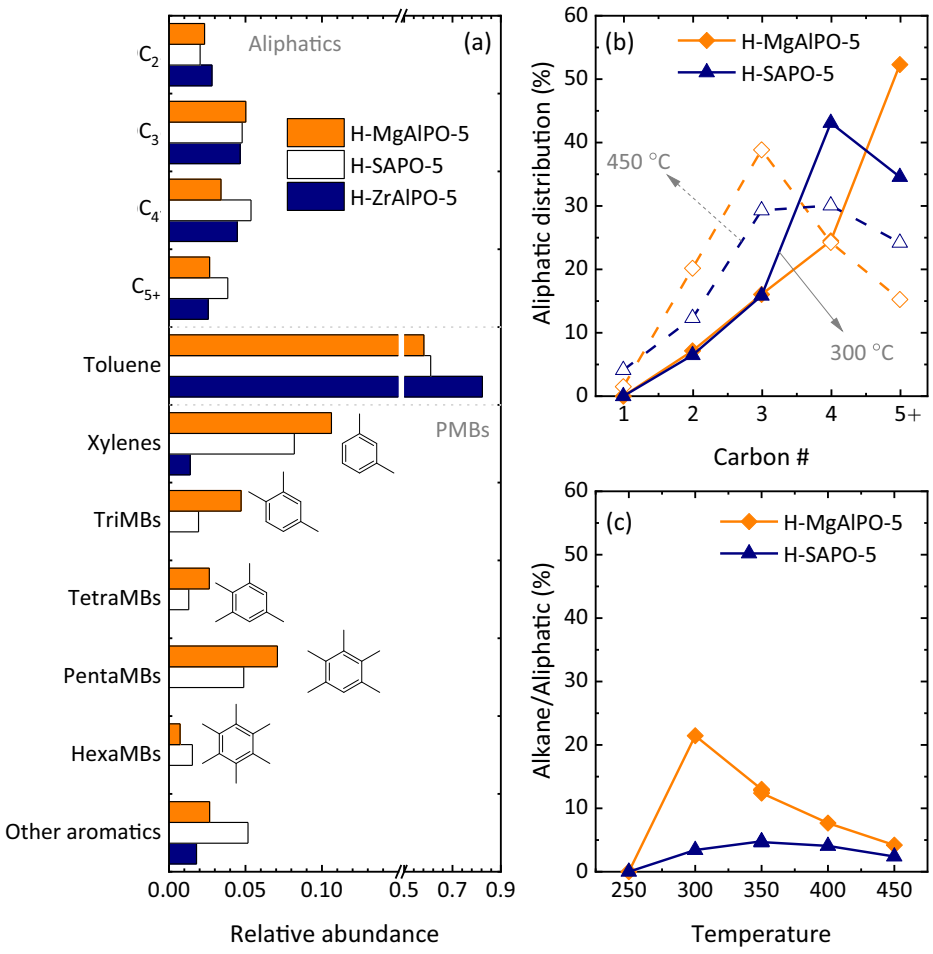

Fig. 5. (a) Reaction product distribution obtained at 400 °C with the H-MeAlPO-5 catalysts and effect of temperature on the (b) aliphatic distribution and (c) alkane-to-aliphatics ratio. GHSV = 34 (H-MgAlPO-5), 26 (H-SAPO-5) and 15 $cm^3\ g^{-1}\ s^{-1}$ (H-ZrAlPO-5). $P_{Benzene}$ = 80 mbar, P_{DME} = 20 mbar.

energy values in this work are estimated within the same range, which confirms the direct role of acid strength in the methylation pathway in a broad range of microporous acidic catalysts. Comparing the sensitivity to the acid strength from these experimental values to those computed before (Fig. 3), the apparent activation energy presents a slope (0.50) much closer to that of DME-benzene co-adsorption energies (0.47) rather than those of intrinsic/apparent activation barriers (0.83 and 0.95, respectively). This result only corroborates the impact of adsorption and diffusion events on the computation of apparent kinetics in a flow reactor.

3.3. Kinetics of benzene methylation with DME

A more in-depth study of benzene methylation was carried out by studying the effect of the partial pressure of each reactant, benzene and DME. Because of the low activity of H-ZrAlPO-5, this study was only performed for the H-MgAlPO-5 and H-SAPO-5 catalysts. Moreover, due to the important contribution of competing reactions at 450 °C, the study was carried out at 300–400 °C. The resulting conversion and selectivity corresponding to these experiments are detailed in **Fig. S9 and S10**. The evolution of the methylation products (Toluene + PMBs) formation rate with benzene partial pressure is depicted in Fig. 7**a and 7c** for a fixed DME partial pressure of 40 mbar. The methylation of benzene follows a (quasi)-first order kinetics in the investigated benzene pressure range. Although the intersection with the Y axis is not exactly 0 at 400 °C, the linear increase of the formation rate with both catalysts is evident. In contrast, regarding the influence of DME partial pressure on the methylation products formation rate, the trends obtained with both catalysts are different (Fig. 7**b and 7d**). The methylation products formation rate decreases for the H-MgAlPO-5 catalyst, but is almost constant for H-SAPO-5 (slight increase at 400 °C). A first order kinetics with respect to benzene and a zero order with respect to DME suggest a fast formation of DME-derived surface species that react with benzene in the rate-determining step [15,18]. This well-established behavior can be assumed for H-SAPO-5 catalyst. However, the decrease in the methylation products formation rate on the H-MgAlPO-5 catalyst upon increasing DME partial pressure may be explained by an entropic effect of a hindered interaction between the reactants, by a decrease in the available sites due to the adsorption of water, or by a promoted reaction between DME and the beforehand formed SMS, as suggested by Wang et al. [97]. Although the role of water in MTH-related reaction is noteworthy, a drastic decrease of the oxygenate conversion is observed when DME partial pressure was increased (**Fig. S9**). For this reason, it is not likely that, in this case, this decreasing trend is directly due to the competitive adsorption of water on the acid sites. On the other hand, a reaction between DME and SMS would mean that a strong competition between benzene and DME could influence the reaction at high DME partial pressures [14], as previously observed at 450 °C (Fig. 3). A competing interaction between benzene and methanol (as methylating agent) to react with the oxygenate- or SMS-covered site was previously observed over micron-sized H-ZSM-5

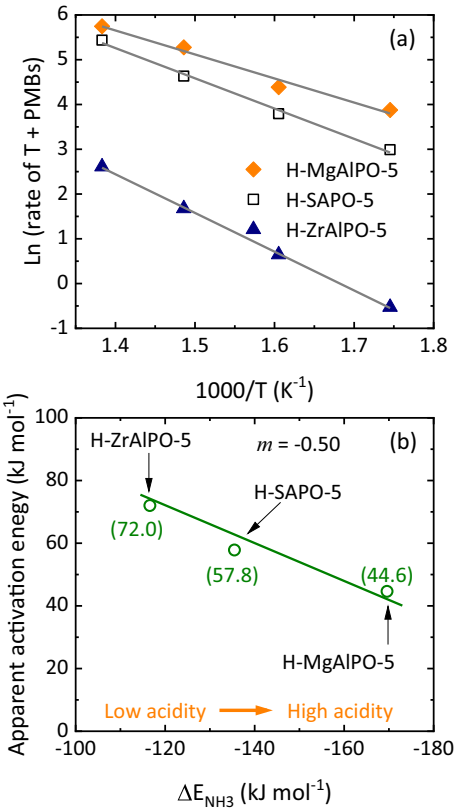

Fig. 6. (a) Temperature correlation for the formation of methylation products during co-feeding reactions of benzene (80 mbar) and DME (20 mbar), and (b) the corresponding evolution with ammonia adsorption energies of the apparent activation energy.

at 250 °C [14]. However, a low, but positive influence of DME pressure on benzene methylation rate was observed over H-ZSM-5 nanosheets at similar temperatures [98]. In those cases, the difference between the two studies could be due to the different methylating agent, to the different diffusion length, or both.

In order to elucidate the role of both reactants in the formation of aliphatics, the evolution of the aliphatic formation rate was also monitored during these experiments and is presented in Fig. 8. Both catalysts show zero order kinetics with respect to benzene partial pressure (Fig. 8**a and 8c**). Therefore, the formation of aliphatics is not affected by the partial pressure of benzene, pointing out that the main source of these compounds should be the evolution of the alkene cycle of the dual cycle mechanism and not the dealkylation of arene-based compounds. The clear decrease in the ratio between the formation rates of aliphatics and methylation products also supports this conclusion (**Figs. S11a and S11b**). An increasing trend is observed for the aliphatic formation rate with increasing DME partial pressure. The H-SAPO-5 catalyst exhibits a quasi-first order kinetics, with an ostensibly higher slope at 400 °C (Fig. 8**d**). According to Wen et al. [19], the stepwise benzene methylation pathway is kinetically favored from this temperature using HZSM-5 and H-beta zeolites. Assuming this is applicable to our materials, it could explain the much faster increase in the aliphatic formation rate observed with the H-SAPO-5 catalyst. Benzene and DME will compete in the reaction with SMS, and this catalyst seems to promote the reaction between DME and SMS.

Otherwise, a Langmuir-Hinshelwood-type evolution of the aliphatic formation rate towards a saturation value is observed for the H-MgAlPO-5 catalyst (Fig. 8**b**). Hill et al. [18] observed this saturation curve for the formation rate of triMBs with respect to xylene partial pressure during the methylation of this aromatic compound over H-ZSM-5. They suggested different possibilities for this behavior: a change in the predominant surface species, a change in the rate-determining step, or diffusion limitations. According to kinetic computations [16], co-adsorbed benzene could play an important role in the reaction at low temperature (ca. 100 °C) and very low partial pressure of the oxygenates (0.2 mbar). At these conditions, SMS would not be the most abundant adsorbed species. Nonetheless, these conditions are far from those employed in our work, where the sequential or stepwise mechanism should be promoted, according to the same authors. In our case, the increase in the aliphatic formation rate (Fig. 8**b**) and the decrease in the methylation products formation rate (Fig. 7**b**) when increasing DME partial pressure up to 80 mbar could be explained by the promotion of competing reactions involving DME and SMS, as observed for the H-SAPO-5 catalyst. However, at a DME partial pressure of 100 mbar, the formation rate of both product families decrease. Therefore, the decreasing trend of the methylation products formation rate with DME pressure (Fig. 7**b**) is more likely explained by diffusion limitations and/or steric hindrance. This can be caused by a stronger adsorption of DME over the acid sites of H-MgAlPO-5 catalyst in the surface reactions, leading for example to the formation of H-bonded DME/

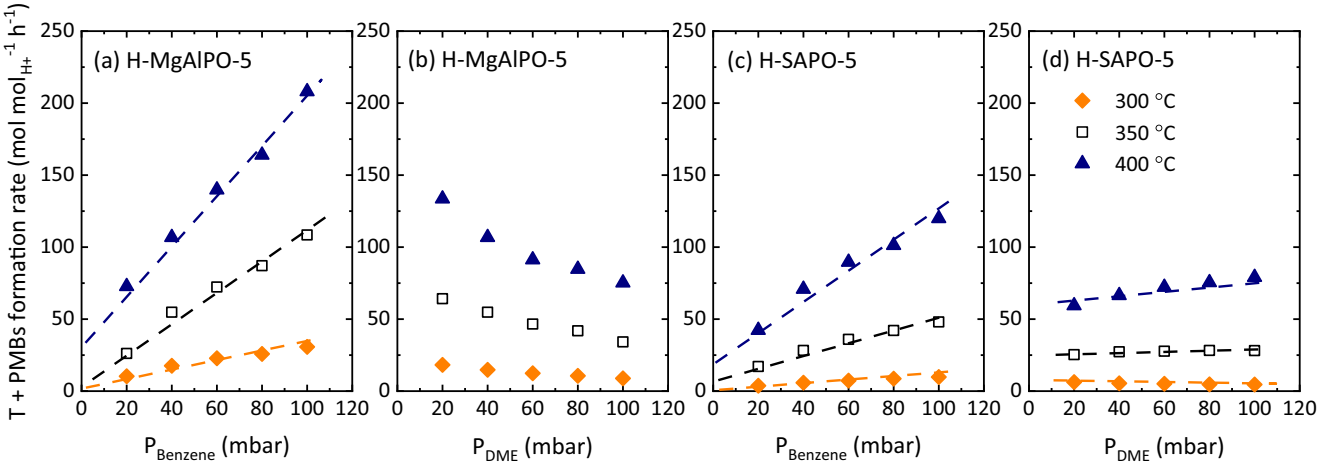

Fig. 7. Evolution with (a, c) benzene (P_{DME} = 40 mbar) and (b, d) DME partial pressure ($P_{Benzene}$ = 40 mbar) of the toluene + PMBs formation rate for the (a, b) H-MgAlPO-5 (GHSV = 33, 53 and 68 cm^3 g^{-1} s^{-1}) and (c, d) H-SAPO-5 catalysts (GHSV = 26, 33 and 34 cm^3 g^{-1} s^{-1}).

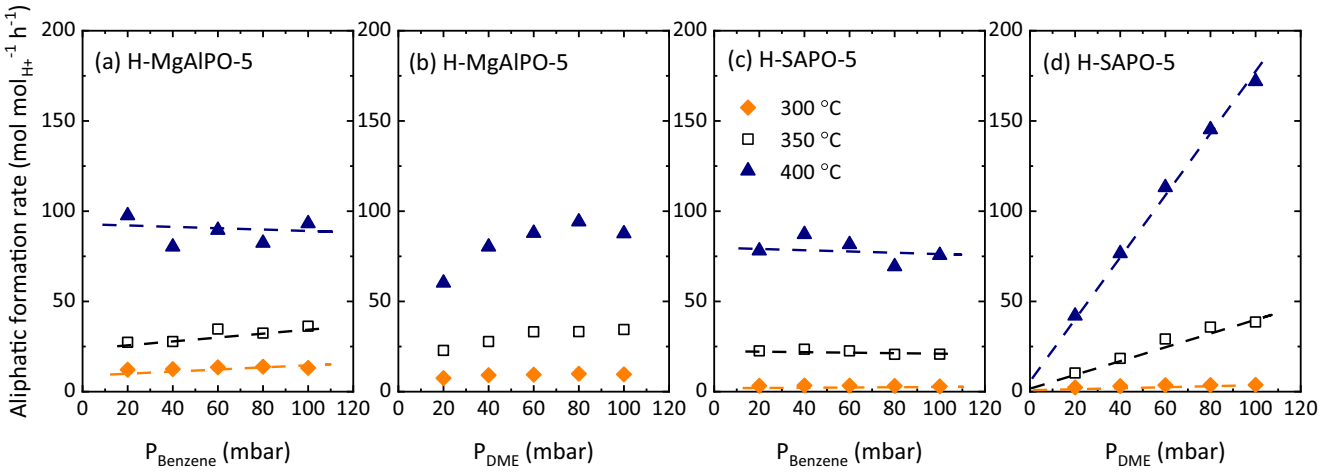

Fig. 8. Evolution with (a, c) benzene (P_{DME} = 40 mbar) and (b, d) DME partial pressure ($P_{Benzene}$ = 40 mbar) of the aliphatic formation rate for the (a, b) H-MgAlPO-5 (GHSV = 33, 53 and 68 cm^3 g^{-1} s^{-1}) and (c, d) H-SAPO-5 catalysts (GHSV = 26, 33 and 34 cm^3 g^{-1} s^{-1}).

methanol clusters in the micropores [99]. Considering the low contact time values used in these experiments, this could occur when the relative amount of DME in the reaction medium is high. Nonetheless, the formation of incipient coke that hinders reactants diffusion cannot be neglected at these conditions of high DME partial pressure, since the important role of DME and methanol in catalyst deactivation is well known in MTH chemistry [100,101]. Likewise, the adsorption of water on the acid sites, leading to a decrease in both formation rates, cannot be ruled out either, despite the significant decrease in oxygenate conversion at high DME partial pressure (**Fig. S9**).

The differences between H-MgAlPO-5 and H-SAPO-5 catalysts are also highlighted by the evolution of conversion in these experiments (**Figs. S9 and S10**). Using either catalysts, the conversion of benzene slightly declines and that of DME increases when the benzene partial pressure is increased. Then, methylation is promoted and the selectivity to toluene increases. However, increasing the partial pressure of DME, the benzene conversion trend is different. It decreases with the H-MgAlPO-5 catalyst, but slightly increases with the H-SAPO-5 catalyst. This, again, supports the different behavior of each catalyst, with a hindered benzene conversion due to the diffusion constraints for the H-MgAlPO-5 catalyst. In any case, the selectivity to aliphatics is clearly promoted at high DME partial pressure, suggesting a disfavored methylation at these conditions with respect to competing secondary reactions. This is especially noticeable in H-SAPO-5 experiments, where the increase in temperature boosts the formation of aliphatics in comparison to methylation routes (**Fig. S11c and S11d**).

Due to the role of aliphatics in the reaction network and the different performance of both catalysts, additional experiments were carried out in order to compare the methylation rate of arenes (using benzene as the model compound) and alkenes (using propene). Experimental runs were performed using different contact time values to estimate the initial formation rate of the primary products (toluene and butenes, respectively). **Fig. S12** shows the evolution with contact time of these formation rates and Table 2 summarizes the initial methylation rate in each case. The estimation of the initial formation rates confirms the highest activity of the H-MgAlPO-5 catalyst, with 372 and 250 mol mol$_{H+}^{-1}$ h^{-1} for the formation rate of toluene and butenes, respectively. The estimated values for H-SAPO-5 catalyst are 128 and 66 mol mol$_{H+}^{-1}$ h^{-1} at 400 °C. The benzene methylation rate is 2.9 times higher using H-MgAlPO-5 catalyst, but interestingly, propene methylation is even faster (3.8 times) over this catalyst. This is translated to ratios between benzene and propene methylations of 1.5 and 1.9 with H-MgAlPO-5 and H-SAPO-5, respectively. Therefore, the H-MgAlPO-5 catalyst is more active not only for methylation of aromatics, but also for a selective methylation of alkenes under these conditions.

Table 2
Initial methylation rate of benzene ($P_{Benzene}$ = 80 mbar, P_{DME} = 20 mbar) and propene ($P_{Propene}$ = 60 mbar, P_{DME} = 60 mbar) over MeAlPO-5 catalysts at 400 °C.

	H-MgAlPO-5	H-SAPO-5	H-MgAlPO-5/ H-SAPO-5
Benzene (mol mol$_{H+}^{-1}$h^{-1})	372	128	2.9
Propene (mol mol$_{H+}^{-1}$h^{-1})	250	66	3.8
Benzene/propene	1.5	1.9	

Considering our findings, it can be surmised that, at those conditions where the direct methylation of aromatics and alkenes competes with other pathways involved in the dual-cycle mechanism, the methylation of hydrocarbons is favored over H-MgAlPO-5, while competing and secondary routes are more favored over H-SAPO-5. Here, one should take into account a promoted reaction between SMS and DME (instead of benzene), the oligomerization and cracking of alkene-cycle intermediates, the dealkylation of arene-cycle intermediates or hydrogen transfer reactions. Based on our results, cracking reactions can be noticeable at high temperatures (Fig. 5) and, although benzene partial pressure seems to play no role in the formation of aliphatics (Fig. 8), it cannot be discarded as a source of aliphatic compounds at high temperature, especially using the H-SAPO-5 catalyst. The high propene methylation activity, observed mainly with the H-MgAlPO-5 catalyst (Table 2), also suggests that other alkene-involved secondary reactions should not be neglected. Thereby, potential routes involving oligomerization and aromatization of long-chained alkenes should take place mostly at high DME concentration in the reaction medium (Fig. 8) and using the most acidic H-MgAlPO-5 catalyst. These conditions of high DME partial pressure, and especially at high temperature, can also induce a fast formation of coke. Although this factor is mostly avoided at the experimental conditions used, the presence of incipient carbon species within the pores of these materials could also explain the diffusion limitations suggested by the above presented results. Despite the clear differences that have been found between the methylation of benzene over this isomorphically substituted H-MeAlPO-5 series of catalysts, the evidence is insufficient for discerning the role of each competing reaction, mostly those involving alkenes. The topology and properties of these materials seems to be suitable for more in-depth future studies on the role of alkenes

in the methylation network. Improving our understanding of these individual reactions involved in the dual-cycle mechanism could play a crucial role to further tune the reaction products and attenuate coke formation, initiated by the arene cycle, in the MTH process.

4. Conclusion

Benzene methylation, as one of the main individual steps of the MTH reaction, has been studied over a series of H-MeAlPO-5 catalysts with a combination of DFT calculations and kinetic measurements. The isomorphous substitution with Mg, Zn, Co, Si, Ti and Zr of these AlPO-5 materials has led to catalysts exhibiting the same AFI topology but with markedly different acid strengths. The catalyst acid strength, quantified by calculating the heat of ammonia adsorption, is demonstrated to have an important effect on the benzene methylation activity. Of all the considered materials, H-MgAlPO-5, the most acidic zeotype, is characterized by the highest adsorption strength of DME and benzene and by the lowest methylation barriers, while H-ZrAlPO-5 with the lowest acid strength is shown to have the lowest methylation activity. Our static DFT calculations clearly demonstrate the existence of an inverse linear relationship between the benzene methylation barriers with DME in the arene cycle and the acid site strength. The direct correlation between the acid strength and the apparent activation energy of benzene methylation has been confirmed by kinetic measurements at operating conditions, with the production of toluene being promoted in the following order: H-MgAlPO-5, H-SAPO-5 and H-ZrAlPO-5. The catalyst with the highest acid strength, H-MgAlPO-5, maximizes toluene formation and also promotes polymethylbenzenes as byproducts.

A (pseudo-)first-order kinetics and a zero-order with respect to benzene partial pressure have been determined for the methylation products and aliphatics formation rates, respectively, when H-MgAlPO-5 or H-SAPO-5 were studied. For H-SAPO-5, the formation rate of methylation products is independent on the DME partial pressure and that of aliphatics follows a linear dependency. These results suggest that aliphatics are mostly formed through competing reactions involved in the dual-cycle mechanism, whose extent is substantially increased upon increasing the relative amount of DME in the reaction medium and promoted with this catalyst. For H-MgAlPO-5, on the other hand, a decreasing trend in methylation products formation rate and a saturating curve were observed for aliphatic formation rates with respect to DME partial pressure, suggesting that diffusion limitations exist when the concentration of this reactant in the reaction medium is high.

Control experiments of propene methylation further suggest that the H-MgAlPO-5 catalyst does not only promote benzene methylation, but also a selective methylation of alkenes. The methylation of benzene is 2.9 times faster over this catalyst compared to H-SAPO-5, whereas propene methylation is 3.8 times faster, at 400 °C. The higher selectivity of H-MgAlPO-5 towards alkene methylation motivates further mechanistic investigations of MTH-relevant reactions within isomorphically substituted MeAlPO materials.

Declaration of Competing Interest

The authors declare that they have no known competing financial interests or personal relationships that could have appeared to influence the work reported in this paper.

Acknowledgements

MM, ER, SS, UO acknowledge the Norwegian Research Council through contracts nr. 239193 (NanoReactor) and 288331 (CO2LO). TC-L acknowledges the Basque Government (IT1218-19) and the Spanish Government for the award of the FPU grant (FPU15-01666) and the additional mobility grant (EST18/00101). P.C. and V.V.S. acknowledge funding from the European Research Council under the ERC Grant Agreement 240483 and the European Union's Horizon 2020 research and innovation programme (Consolidator ERC Grant Agreement 647755—DYNPOR). V.V.S. thanks the Research Board of the Ghent University for funding. Computational resources and services were provided by the VSC (Flemish Supercomputer Center), funded by the Research Foundation Flanders (FWO) and the Flemish Government—department EWI.

Appendix A. Supplementary material

Supplementary data to this article can be found online at https://doi.org/10.1016/j.jcat.2021.11.002.

References

[1] M.C. Clark, C.M. Smith, D.L. Stern, J.S. Beck, Alkylation of Aromatics, in: Handb. Heterog. Catal., Wiley-VCH Verlag GmbH & Co. KGaA, 2008, pp. 3153–3168. https://doi.org/10.1002/9783527610044.hetcat0159.
[2] S. Svelle, M. Visur, U. Olsbye, Saepurahman, M. Bjørgen, Mechanistic aspects of the zeolite catalyzed methylation of alkenes and aromatics with methanol: a review, Top. Catal. 54 (13-15) (2011) 897–906, https://doi.org/10.1007/s11244-011-9697-7.
[3] I. Dimitriou, H. Goldingay, A.V. Bridgwater, Techno-economic and uncertainty analysis of Biomass to Liquid (BTL) systems for transport fuel production, Renew. Sustain. Energy Rev. 88 (2018) 160–175, https://doi.org/10.1016/j.rser.2018.02.023.
[4] I. Yarulina, A.D. Chowdhury, F. Meirer, B.M. Weckhuysen, J. Gascon, Recent trends and fundamental insights in the methanol-to-hydrocarbons process, Nat. Catal. 1 (6) (2018) 398–411, https://doi.org/10.1038/s41929-018-0078-5.
[5] D. Rojo-Gama, M. Signorile, F. Bonino, S. Bordiga, U. Olsbye, K.P. Lillerud, P. Beato, S. Svelle, Structure–deactivation relationships in zeolites during the methanol–to-hydrocarbons reaction: complementary assessments of the coke content, J. Catal. 351 (2017) 33–48, https://doi.org/10.1016/j.jcat.2017.04.015.
[6] I. Yarulina, K. De Wispelaere, S. Bailleul, J. Goetze, M. Radersma, E. Abou-Hamad, I. Vollmer, M. Goesten, B. Mezari, E.J.M. Hensen, J.S. Martínez-Espín, M. Morten, S. Mitchell, J. Perez-Ramirez, U. Olsbye, B.M. Weckhuysen, V. Van Speybroeck, F. Kapteijn, J. Gascon, Structure–performance descriptors and the role of Lewis acidity in the methanol-to-propylene process, Nat. Chem. 10 (8) (2018) 804–812, https://doi.org/10.1038/s41557-018-0081-0.
[7] P. Tian, Y. Wei, M. Ye, Z. Liu, Methanol to olefins (MTO): from fundamentals to commercialization, ACS Catal. 5 (3) (2015) 1922–1938, https://doi.org/10.1021/acscatal.5b00007.
[8] N. Chen, W. Reagan, Evidence of autocatalysis in methanol to hydrocarbon reactions over zeolite catalysts, J. Catal. 59 (1) (1979) 123–129, https://doi.org/10.1016/S0021-9517(79)80050-0.
[9] I.M. Dahl, S. Kolboe, On the reaction mechanism for hydrocarbon formation from methanol over SAPO-34, J. Catal. 149 (2) (1994) 458–464.
[10] M. Bjorgen, S. Svelle, F. Joensen, J. Nerlov, S. Kolboe, F. BONINO, L. Palumbo, S. Bordiga, U. Olsbye, Conversion of methanol to hydrocarbons over zeolite H-ZSM-5: On the origin of the olefinic species, J. Catal. 249 (2) (2007) 195–207, https://doi.org/10.1016/j.jcat.2007.04.006.
[11] M. Westgård Erichsen, M. Mortén, S. Svelle, O. Sekiguchi, E. Uggerud, U. Olsbye, Conclusive evidence for two unimolecular pathways to zeolite-catalyzed de-alkylation of the heptamethylbenzenium cation, ChemCatChem. 7 (24) (2015) 4143–4147, https://doi.org/10.1002/cctc.201500793.
[12] J.S. Martínez-Espín, K. De Wispelaere, T.V.W. Janssens, S. Svelle, K.P. Lillerud, P. Beato, V. Van Speybroeck, U. Olsbye, Hydrogen transfer versus methylation: on the genesis of aromatics formation in the methanol-to-hydrocarbons reaction over H-ZSM-5, ACS Catal. 7 (9) (2017) 5773–5780, https://doi.org/10.1021/acscatal.7b0164310.1021/acscatal.7b01643.s001.
[13] W.U. Wen, S. Yu, C. Zhou, H. Ma, Z. Zhou, C. Cao, J. Yang, M. Xu, F. Qi, G. Zhang, Y. Pan, Formation and fate of formaldehyde in methanol-to-hydrocarbon reaction: In situ synchrotron radiation photoionization mass spectrometry study, Angew. Chemie - Int. Ed. 59 (12) (2020) 4873–4878, https://doi.org/10.1002/anie.v59.1210.1002/anie.201914953.
[14] J.S. Martinez-Espin, K. De Wispelaere, M. Westgård Erichsen, S. Svelle, T.V.W. Janssens, V. Van Speybroeck, P. Beato, U. Olsbye, Benzene co-reaction with methanol and dimethyl ether over zeolite and zeotype catalysts: Evidence of

parallel reaction paths to toluene and diphenylmethane, J. Catal. 349 (2017) 136–148, https://doi.org/10.1016/j.jcat.2017.03.007.
[15] J. Van Der Mynsbrugge, M. Visur, U. Olsbye, P. Beato, M. Bjorgen, V. Van Speybroeck, S. Svelle, Methylation of benzene by methanol: Single-site kinetics over H-ZSM-5 and H-beta zeolite catalysts, J. Catal. 292 (2012) 201–212, https://doi.org/10.1016/j.jcat.2012.05.015.
[16] M. DeLuca, P. Kravchenko, A. Hoffman, D. Hibbitts, Mechanism and kinetics of methylating C6–C12 methylbenzenes with methanol and dimethyl ether in H-MFI zeolites, ACS Catal. 9 (7) (2019) 6444–6460, https://doi.org/10.1021/acscatal.9b0065010.1021/acscatal.9b00650.s001.
[17] Saepurahman, M. Visur, U. Olsbye, M. Bjørgen, S. Svelle, Svelle, In situ FT-IR mechanistic investigations of the zeolite catalyzed methylation of benzene with methanol: H-ZSM-5 versus H-beta, Top. Catal. 54 (16-18) (2011) 1293–1301, https://doi.org/10.1007/s11244-011-9751-5.
[18] I. Hill, A. Malek, A. Bhan, Kinetics and mechanism of benzene, toluene, and xylene methylation over H-MFI, ACS Catal. 3 (9) (2013) 1992–2001, https://doi.org/10.1021/cs400377b.
[19] Z. Wen, H. Zhu, X. Zhu, Density functional theory study of the zeolite-catalyzed methylation of benzene with methanol, Catal. Lett. 150 (1) (2020) 21–30, https://doi.org/10.1007/s10562-019-02931-3.
[20] S. Svelle, S. Kolboe, O. Swang, U. Olsbye, Methylation of alkenes and methylbenzenes by dimethyl ether or methanol on acidic zeolites, J. Phys. Chem. B. 109 (26) (2005) 12874–12878, https://doi.org/10.1021/jp051125z10.1021/jp051125z.s001.
[21] U. Olsbye, S. Svelle, M. Bjørgen, P. Beato, T.V.W. Janssens, F. Joensen, S. Bordiga, K.P. Lillerud, Conversion of methanol to hydrocarbons: How zeolite cavity and pore size controls product selectivity, Angew. Chemie - Int. Ed. 51 (24) (2012) 5810–5831, https://doi.org/10.1002/anie.201103657.
[22] J. Li, Y. Wei, G. Liu, Y. Qi, P. Tian, B. Li, Y. He, Z. Liu, Comparative study of MTO conversion over SAPO-34, H-ZSM-5 and H-ZSM-22: Correlating catalytic performance and reaction mechanism to zeolite topology, Catal. Today. 171 (1) (2011) 221–228, https://doi.org/10.1016/j.cattod.2011.02.027.
[23] M. Gao, H. Li, M. Yang, J. Zhou, X. Yuan, P. Tian, M. Ye, Z. Liu, A modeling study on reaction and diffusion in MTO process over SAPO-34 zeolites, Chem. Eng. J. 377 (2019) 119668, https://doi.org/10.1016/j.cej.2018.08.054.
[24] W. Dai, G. Wu, L. Li, N. Guan, M. Hunger, Mechanisms of the deactivation of SAPO-34 materials with different crystal sizes applied as MTO catalysts, ACS Catal. 3 (4) (2013) 588–596, https://doi.org/10.1021/cs400007v.
[25] P. Ferri, C. Li, R. Millán, J. Martínez-Triguero, M. Moliner, M. Boronat, A. Corma, Impact of zeolite framework composition and flexibility on methanol-to-olefins selectivity: confinement or diffusion?, Angew Chemie - Int. Ed. 59 (44) (2020) 19708–19715, https://doi.org/10.1002/anie.v59.4410.1002/anie.202007609.
[26] P. Cnudde, R. Demuynck, S. Vandenbrande, M. Waroquier, G. Sastre, V.V. Speybroeck, Light olefin diffusion during the MTO process on H-SAPO-34: a complex interplay of molecular factors, J. Am. Chem. Soc. 142 (13) (2020) 6007–6017, https://doi.org/10.1021/jacs.9b1024910.1021/jacs.9b10249.s001.
[27] P. Cnudde, E.A. Redekop, W. Dai, N.G. Porcaro, M. Waroquier, S. Bordiga, M. Hunger, L. Li, U. Olsbye, V. Van Speybroeck, Experimental and Theoretical Evidence for the Promotional Effect of Acid Sites on the Diffusion of Alkenes through Small-Pore Zeolites, Angew. Chemie - Int. Ed. 60 (18) (2021) 10016–10022, https://doi.org/10.1002/anie.v60.1810.1002/anie.202017025.
[28] L. Qi, J. Li, L. Wang, L. Xu, Z. Liu, Unusual deactivation of HZSM-5 zeolite in the methanol to hydrocarbon reaction, Catal Sci. Technol. 7 (4) (2017) 894–901, https://doi.org/10.1039/C6CY02459A.
[29] X. Jiang, X. Su, X. Bai, Y. Li, L. Yang, K. Zhang, Y. Zhang, Y. Liu, W. Wu, Conversion of methanol to light olefins over nanosized [Fe, Al]ZSM-5 zeolites: influence of Fe incorporated into the framework on the acidity and catalytic performance, Microporous Mesoporous Mater. 263 (2018) 243–250, https://doi.org/10.1016/j.micromeso.2017.12.029.
[30] P. Pérez-Uriarte, M. Gamero, A. Ateka, M. Díaz, A.T. Aguayo, J. Bilbao, Effect of the acidity of HZSM-5 zeolite and the binder in the DME transformation to olefins, Ind. Eng. Chem. Res. 55 (6) (2016) 1513–1521, https://doi.org/10.1021/acs.iecr.5b0447710.1021/acs.iecr.5b04477.s001.
[31] M. Mortén, Ł. Mentel, A. Lazzarini, I.A. Pankin, C. Lamberti, S. Bordiga, V. Crocellà, S. Svelle, K.P. Lillerud, U. Olsbye, A systematic study of isomorphically substituted H-MAlPO-5 materials for the methanol-to-hydrocarbons reaction, ChemPhysChem. 19 (4) (2018) 484–495, https://doi.org/10.1002/cphc.201701024.
[32] G. Müller, J. Bódis, G. Eder-Mirth, J. Kornatowski, J.A. Lercher, In situ FT-IR microscopic investigation of metal substituted AlPO4-5 single crystals, J. Mol. Struct. 410–411 (1997) 173–178, https://doi.org/10.1016/S0022-2860(96)09578-6.
[33] M. Popova, C. Minchev, V. Kanazirev, Effect of the different modifications of AlPO-5 molecular sieve on its acidity and catalytic properties in methanol conversion to hydrocarbons, React. Kinet. Catal. Lett. 63 (1998) 379–384, https://doi.org/10.1007/BF02475415.
[34] M.K. Dongare, D.P. Sabde, R.A. Shaikh, K.R. Kamble, S.G. Hegde, Synthesis, characterization and catalytic properties of ZrAPO-5, Catal. Today. 49 (1-3) (1999) 267–276, https://doi.org/10.1016/S0920-5861(98)00433-7.
[35] B.M. Weckhuysen, R.R. Rao, J.A. Martens, R.A. Schoonheydt, Transition metal ions in microporous crystalline aluminophosphates: Isomorphous substitution, Eur. J. Inorg. Chem. (1999) 565–577, https://doi.org/10.1002/(SICI)1099-0682(199904)1999:4<565::AID-EJIC565>3.0.CO;2-Y.
[36] L. Feng, X. Qi, J. Li, Y. Zhu, L. Zhu, Synthesis of MgAPO-5 molecular sieves and their kinetic behavior for n-hexane cracking, React. Kinet. Catal. Lett. 98 (2) (2009) 327–339, https://doi.org/10.1007/s11144-009-0078-1.
[37] M. Westgård Erichsen, S. Svelle, U. Olsbye, H-SAPO-5 as methanol-to-olefins (MTO) model catalyst: towards elucidating the effects of acid strength, J. Catal. 298 (2013) 94–101, https://doi.org/10.1016/j.jcat.2012.11.004.
[38] S.-H. Zhang, C.-M. Wang, X.-G. Zhou, Y.-A. Zhu, Elucidating the methanol conversion in H-SAPO-5 from first principles: nature of hydrocarbon pool and scission style, Mol. Catal. 490 (2020) 110948, https://doi.org/10.1016/j.mcat.2020.110948.
[39] M. García Ruiz, D.A. Solís Casados, J. Aguilar Pliego, C. Márquez Álvarez, E. Sastre de Andrés, D. Sanjurjo Tartalo, M. Sanchez-Sanchez, M. Grande Casas, Synthesis and characterization of aluminophosphates Type-5 and 36 doubly modified with Si and Zn and its catalytic application in the reaction of methanol to hydrocarbons (MTH), Top. Catal. 63 (5-6) (2020) 437–450, https://doi.org/10.1007/s11244-020-01266-3.
[40] C.M. Wang, R.Y. Brogaard, B.M. Weckhuysen, J.K. Nørskov, F. Studt, Reactivity descriptor in solid acid catalysis: Predicting turnover frequencies for propene methylation in zeotypes, J. Phys. Chem. Lett. 5 (2014) 1516–1521. https://doi.org/dx.doi.org/10.1021/jz500482z |.
[41] R.Y. Brogaard, C.-M. Wang, F. Studt, Methanol-alkene reactions in zeotype acid catalysts: Insights from a descriptor-based approach and microkinetic modeling, ACS Catal. 4 (12) (2014) 4504–4509, https://doi.org/10.1021/cs5014267.
[42] C.-M. Wang, R.Y. Brogaard, Z.-K. Xie, F. Studt, Transition-state scaling relations in zeolite catalysis: influence of framework topology and acid-site reactivity, Catal. Sci. Technol. 5 (5) (2015) 2814–2820, https://doi.org/10.1039/C4CY01692K.
[43] M. Westgård Erichsen, S. Svelle, U. Olsbye, The influence of catalyst acid strength on the methanol to hydrocarbons (MTH) reaction, Catal. Today. 215 (2013) 216–223, https://doi.org/10.1016/j.cattod.2013.03.017.
[44] M. Westgård Erichsen, K. De Wispelaere, K. Hemelsoet, S.L.C. Moors, T. Deconinck, M. Waroquier, S. Svelle, V. Van Speybroeck, U. Olsbye, How zeolitic acid strength and composition alter the reactivity of alkenes and aromatics towards methanol Dedicated to the memory of Haldor Topsøe, J. Catal. 328 (2015) 186–196, https://doi.org/10.1016/j.jcat.2015.01.013.
[45] G. Kresse, J. Hafner, Ab initio molecular dynamics for liquid metals, Phys. Rev. B. 47 (1) (1993) 558–561, https://doi.org/10.1103/PhysRevB.47.558.
[46] G. Kresse, J. Hafner, Ab initio molecular-dynamics simulation of the liquid-metal–amorphous-semiconductor transition in germanium, Phys. Rev. B. 49 (20) (1994) 14251–14269, https://doi.org/10.1103/PhysRevB.49.14251.
[47] G. Kresse, J. Furthmüller, Efficient iterative schemes for ab initio total-energy calculations using a plane-wave basis set, Phys. Rev. B. 54 (16) (1996) 11169–11186, https://doi.org/10.1103/PhysRevB.54.11169.
[48] G. Kresse, J. Furthmüller, Efficiency of ab-initio total energy calculations for metals and semiconductors using a plane-wave basis set, Comput. Mater. Sci. 6 (1) (1996) 15–50, https://doi.org/10.1016/0927-0256(96)00008-0.
[49] J.P. Perdew, K. Burke, M. Ernzerhof, Generalized gradient approximation made simple, Phys. Rev. Lett. 77 (18) (1996) 3865–3868, https://doi.org/10.1103/PhysRevLett.77.3865.
[50] S. Grimme, J. Antony, S. Ehrlich, H. Krieg, A consistent and accurate ab initio parametrization of density functional dispersion correction (DFT-D) for the 94 elements H-Pu, J. Chem. Phys. 132 (15) (2010) 154104, https://doi.org/10.1063/1.3382344.
[51] G. Kresse, D. Joubert, From ultrasoft pseudopotentials to the projector augmented-wave method, Phys. Rev. B. 59 (3) (1999) 1758–1775, https://doi.org/10.1103/PhysRevB.59.1758.
[52] P.E. Blöchl, Projector augmented-wave method, Phys. Rev. B. 50 (24) (1994) 17953–17979, https://doi.org/10.1103/PhysRevB.50.17953.
[53] K. Lejaeghere, G. Bihlmayer, T. Björkman, P. Blaha, S. Blügel, V. Blum, D. Caliste, I.E. Castelli, S.J. Clark, A.D. Corso, S. de Gironcoli, T. Deutsch, J.K. Dewhurst, I. Di Marco, C. Draxl, M. Dułak, O. Eriksson, J.A. Flores-Livas, K.F. Garrity, L. Genovese, P. Giannozzi, M. Giantomassi, S. Goedecker, X. Gonze, O. Grånäs, E.K.U. Gross, A. Gulans, F. Gygi, D.R. Hamann, P.J. Hasnip, N.A.W. Holzwarth, D. Iuşan, D.B. Jochym, F. Jollet, D. Jones, G. Kresse, K. Koepernik, E. Küçükbenli, Y.O. Kvashnin, I.L.M. Locht, S. Lubeck, M. Marsman, N. Marzari, U. Nitzsche, L. Nordström, T. Ozaki, L. Paulatto, C.J. Pickard, W. Poelmans, M.I.J. Probert, K. Refson, M. Richter, G.-M. Rignanese, S. Saha, M. Scheffler, M. Schlipf, K. Schwarz, S. Sharma, F. Tavazza, P. Thunström, A. Tkatchenko, M. Torrent, D. Vanderbilt, M.J. van Setten, V. Van Speybroeck, J.M. Wills, J.R. Yates, G.-X. Zhang, S. Cottenier, Reproducibility in density functional theory calculations of solids, Science 351 (2016) aad3000, https://doi.org/10.1126/SCIENCE.AAD3000.
[54] A. Heyden, A.T. Bell, F.J. Keil, Efficient methods for finding transition states in chemical reactions: comparison of improved dimer method and partitioned rational function optimization method, J. Chem. Phys. 123 (22) (2005) 224101, https://doi.org/10.1063/1.2104507.
[55] M.T. Reetz, A. Meiswinkel, G. Mehler, K. Angermund, M. Graf, W. Thiel, R. Mynott, D.G. Blackmond, Why are BINOL-based monophosphites such efficient ligands in Rh-catalyzed asymmetric olefin hydrogenation?, J Am. Chem. Soc. 127 (2005) 10305–10313, https://doi.org/10.1021/JA052025.
[56] A. Ghysels, D. Van Neck, V. Van Speybroeck, T. Verstraelen, M. Waroquier, Vibrational modes in partially optimized molecular systems, J. Chem. Phys. 126 (22) (2007) 224102, https://doi.org/10.1063/1.2737444.
[57] P.J. Donoghue, P. Helquist, P.-O. Norrby, O. Wiest, Development of a Q2MM force field for the asymmetric rhodium catalyzed hydrogenation of enamides,

J. Chem. Theory Comput. 4 (8) (2008) 1313–1323, https://doi.org/10.1021/ct800132a.
[58] A.n. Ghysels, T. Verstraelen, K. Hemelsoet, M. Waroquier, V. Van Speybroeck, TAMkin: a versatile package for vibrational analysis and chemical kinetics, J. Chem. Inf. Model. 50 (9) (2010) 1736–1750, https://doi.org/10.1021/ci100099g.
[59] D.E.P. Vanpoucke, K. Lejaeghere, V. Van Speybroeck, M. Waroquier, A.n. Ghysels, Mechanical properties from periodic plane wave quantum mechanical codes: the challenge of the flexible nanoporous MIL-47(V) framework, J. Phys. Chem. C. 119 (41) (2015) 23752–23766, https://doi.org/10.1021/acs.jpcc.5b06809.
[60] Y. Zhang, W. Yang, Comment on "Generalized Gradient Approximation Made Simple," Phys. Rev. Lett. 80 (1998) 890. https://doi.org/10.1103/PhysRevLett.80.890.
[61] J. VandeVondele, M. Krack, F. Mohamed, M. Parrinello, T. Chassaing, J. Hutter, Quickstep: Fast and accurate density functional calculations using a mixed Gaussian and plane waves approach, Comput. Phys. Commun. 167 (2) (2005) 103–128, https://doi.org/10.1016/j.cpc.2004.12.014.
[62] J. Hutter, M. Iannuzzi, F. Schiffmann, J. VandeVondele, cp2k: atomistic simulations of condensed matter systems, Wiley Interdiscip. Rev. Comput. Mol. Sci. 4 (2014) 15–25, https://doi.org/10.1002/WCMS.1159.
[63] G. Lippert, J. Hutter, M. Parrinello, A hybrid Gaussian and plane wave density functional scheme, Mol. Phys. 92 (1997) 477–488, https://doi.org/10.1080/002689797170220.
[64] G. Lippert, J. Hutter, M. Parrinello, The Gaussian and augmented-plane-wave density functional method for ab initio molecular dynamics simulations, Theor. Chem. Acc. 103 (2) (1999) 124–140, https://doi.org/10.1007/s002140050523.
[65] S. Goedecker, M. Teter, J. Hutter, Separable dual-space Gaussian pseudopotentials, Phys. Rev. B. 54 (3) (1996) 1703–1710, https://doi.org/10.1103/PhysRevB.54.1703.
[66] C. Hartwigsen, S. Goedecker, J. Hutter, Relativistic separable dual-space Gaussian pseudopotentials from H to Rn, Phys. Rev. B. 58 (7) (1998) 3641–3662, https://doi.org/10.1103/PhysRevB.58.3641.
[67] J. VandeVondele, J. Hutter, Gaussian basis sets for accurate calculations on molecular systems in gas and condensed phases, J. Chem. Phys. 127 (11) (2007) 114105, https://doi.org/10.1063/1.2770708.
[68] S. Nosé, A molecular dynamics method for simulations in the canonical ensemble, Mol. Phys. 52 (2) (1984) 255–268, https://doi.org/10.1080/00268978400101201.
[69] G.J. Martyna, M.L. Klein, M. Tuckerman, Nosé-Hoover chains: The canonical ensemble via continuous dynamics, J. Chem. Phys. 97 (4) (1992) 2635–2643, https://doi.org/10.1063/1.463940.
[70] G.J. Martyna, D.J. Tobias, M.L. Klein, Constant pressure molecular dynamics algorithms, J. Chem. Phys. 101 (5) (1994) 4177–4189, https://doi.org/10.1063/1.467468.
[71] I. Kustanovich, D. Goldfarb, Sorption of water, methanol, and ammonia on AlPO4-5 as studied by multinuclear NMR spectroscopy, J. Phys. Chem. 95 (22) (1991) 8818–8823, https://doi.org/10.1021/j100175a073.
[72] P. Borges, R. Ramos Pinto, M.A.N.D.A. Lemos, F. Lemos, J.C. Védrine, E.G. Derouane, F. Ramôa Ribeiro, Activity–acidity relationship for alkane cracking over zeolites: n-hexane cracking over HZSM-5, J. Mol. Catal. A Chem. 229 (1-2) (2005) 127–135, https://doi.org/10.1016/j.molcata.2004.11.012.
[73] N. Katada, S. Sota, N. Morishita, K. Okumura, M. Niwa, Relationship between activation energy and pre-exponential factor normalized by the number of Brønsted acid sites in cracking of short chain alkanes on zeolites, Catal. Sci. Technol. 5 (3) (2015) 1864–1869, https://doi.org/10.1039/C4CY01483A.
[74] C. Liu, I. Tranca, R.A. van Santen, E.J.M. Hensen, E.A. Pidko, Scaling relations for acidity and reactivity of zeolites, J. Phys. Chem. C. 121 (42) (2017) 23520–23530, https://doi.org/10.1021/acs.jpcc.7b08176.
[75] V. Van Speybroeck, K. Hemelsoet, L. Joos, M. Waroquier, R.G. Bell, C.R.A. Catlow, Advances in theory and their application within the field of zeolite chemistry, Chem. Soc. Rev. 44 (20) (2015) 7044–7111, https://doi.org/10.1039/C5CS00029G.
[76] L. Grajciar, C.J. Heard, A.A. Bondarenko, M.V. Polynski, J. Meeprasert, E.A. Pidko, P. Nachtigall, Towards operando computational modeling in heterogeneous catalysis, Chem. Soc. Rev. 47 (22) (2018) 8307–8348, https://doi.org/10.1039/C8CS00398J.
[77] J. Amsler, P.N. Plessow, F. Studt, T. Bučko, Anharmonic correction to adsorption free energy from DFT-based MD using thermodynamic integration, J. Chem. Theory Comput. 17 (2) (2021) 1155–1169, https://doi.org/10.1021/acs.jctc.0c0102210.1021/acs.jctc.0c01022.s001.
[78] A. Bajpai, P. Mehta, K. Frey, A.M. Lehmer, W.F. Schneider, Benchmark first-principles calculations of adsorbate free energies, ACS Catal. 8 (3) (2018) 1945–1954, https://doi.org/10.1021/acscatal.7b03438.
[79] A.J. Jones, E. Iglesia, Kinetic, spectroscopic, and theoretical assessment of associative and dissociative methanol dehydration routes in zeolites, Angew. Chemie Int. Ed. 53 (45) (2014) 12177–12181, https://doi.org/10.1002/anie.201406823.
[80] M.N. Mazar, S. Al-Hashimi, A. Bhan, M. Cococcioni, Methylation of ethene by surface methoxides: a periodic PBE+D study across zeolites, J. Phys. Chem. C. 116 (36) (2012) 19385–19395, https://doi.org/10.1021/jp306003e.
[81] R.Y. Brogaard, R. Henry, Y. Schuurman, A.J. Medford, P.G. Moses, P. Beato, S. Svelle, J.K. Nørskov, U. Olsbye, Methanol-to-hydrocarbons conversion: The alkene methylation pathway, J. Catal. 314 (2014) 159–169, https://doi.org/10.1016/J.JCAT.2014.04.006.
[82] D.A. Simonetti, R.T. Carr, E. Iglesia, Acid strength and solvation effects on methylation, hydride transfer, and isomerization rates during catalytic homologation of C1 species, J. Catal. 285 (1) (2012) 19–30, https://doi.org/10.1016/j.jcat.2011.09.007.
[83] S. Bailleul, K. Dedecker, P. Cnudde, L. Vanduyfhuys, M. Waroquier, V. Van Speybroeck, Ab initio enhanced sampling kinetic study on MTO ethene methylation reaction, J. Catal. 388 (2020) 38–51, https://doi.org/10.1016/J.JCAT.2020.04.015.
[84] P. Cnudde, K. De Wispelaere, J. Van der Mynsbrugge, M. Waroquier, V. Van Speybroeck, Effect of temperature and branching on the nature and stability of alkene cracking intermediates in H-ZSM-5, J. Catal. 345 (2017) 53–69, https://doi.org/10.1016/J.JCAT.2016.11.010.
[85] P. Cnudde, K. De Wispelaere, L. Vanduyfhuys, R. Demuynck, J. Van der Mynsbrugge, M. Waroquier, V. Van Speybroeck, How chain length and branching influence the alkene cracking reactivity on H-ZSM-5, ACS Catal. 8 (10) (2018) 9579–9595, https://doi.org/10.1021/acscatal.8b0177910.1021/acscatal.8b01779.s001.
[86] J. Rey, P. Raybaud, C. Chizallet, T. Bučko, Competition of secondary versus tertiary carbenium routes for the Type B isomerization of Alkenes over acid zeolites quantified by ab initio molecular dynamics Simulations, ACS Catal. 9 (11) (2019) 9813–9828, https://doi.org/10.1021/acscatal.9b02856.
[87] Y. Chen, X. Zhao, Z. Qin, S. Wang, Z. Wei, J. Li, M. Dong, J. Wang, W. Fan, Insight into the methylation of alkenes and aromatics with methanol over zeolite catalysts by linear scaling relations, J. Phys. Chem. C. 124 (25) (2020) 13789–13798, https://doi.org/10.1021/acs.jpcc.0c03405.
[88] D. Lesthaeghe, B. De Sterck, V. Van Speybroeck, G. Marin, M. Waroquier, Zeolite shape-selectivity in the gem-methylation of aromatic hydrocarbons, Angew. Chemie - Int. Ed. 46 (8) (2007) 1311–1314, https://doi.org/10.1002/anie.200604309.
[89] M. Fečík, P.N. Plessow, F. Studt, A systematic study of methylation from benzene to hexamethylbenzene in H-SSZ-13 using density functional theory and ab initio calculations, ACS Catal. 10 (15) (2020) 8916–8925, https://doi.org/10.1021/acscatal.0c02037.
[90] C. Wang, J. Xu, G. Qi, Y. Gong, W. Wang, P. Gao, Q. Wang, N. Feng, X. Liu, F. Deng, Methylbenzene hydrocarbon pool in methanol-to-olefins conversion over zeolite H-ZSM-5, J. Catal. 332 (2015) 127–137, https://doi.org/10.1016/j.jcat.2015.10.001.
[91] L.F. Lin, S.F. Zhao, D.W. Zhang, H. Fan, Y.M. Liu, M.Y. He, Acid strength controlled reaction pathways for the catalytic cracking of 1-pentene to propene over ZSM-5, ACS Catal. 5 (7) (2015) 4048–4059, https://doi.org/10.1021/cs501967r.
[92] A. Miyaji, Y. Sakamoto, Y. Iwase, T. Yashima, R. Koide, K. Motokura, T. Baba, Selective production of ethylene and propylene via monomolecular cracking of pentene over proton-exchanged zeolites: pentene cracking mechanism determined by spatial volume of zeolite cavity, J. Catal. 302 (2013) 101–114, https://doi.org/10.1016/j.jcat.2013.02.013.
[93] C. Ahoba-Sam, M.W. Erichsen, U. Olsbye, Ethene and butene oligomerization over isostructural H-SAPO-5 and H-SSZ-24: Kinetics and mechanism, Chinese J. Catal. 40 (11) (2019) 1766–1777, https://doi.org/10.1016/S1872-2067(19)63426-1.
[94] X. Sun, S. Mueller, Y. Liu, H. Shi, G.L. Haller, M. Sanchez-Sanchez, A.C. Van Veen, J.A. Lercher, On reaction pathways in the conversion of methanol to hydrocarbons on HZSM-5, J. Catal. 317 (2014) 185–197, https://doi.org/10.1016/j.jcat.2014.06.017.
[95] M. Dyballa, U. Obenaus, M. Blum, W. Dai, Alkali metal ion exchanged ZSM-5 catalysts: on acidity and methanol-to-olefin performance, Catal Sci. Technol. 8 (17) (2018) 4440–4449, https://doi.org/10.1039/C8CY01032C.
[96] H.u. Li, X.-G. Li, W.-D. Xiao, Collaborative effect of zinc and phosphorus on the modified HZSM-5 zeolites in the conversion of methanol to aromatics, Catal. Lett. 151 (4) (2021) 955–965, https://doi.org/10.1007/s10562-020-03360-3.
[97] Q. Wang, W. Han, J. Lyu, Q. Zhang, L. Guo, X. Li, In situ encapsulation of platinum clusters within H-ZSM-5 zeolite for highly stable benzene methylation catalysis, Catal. Sci. Technol. 7 (24) (2017) 6140–6150, https://doi.org/10.1039/C7CY01270E.
[98] K. De Wispelaere, J.S. Martínez-Espín, M.J. Hoffmann, S. Svelle, U. Olsbye, T. Bligaard, Understanding zeolite-catalyzed benzene methylation reactions by methanol and dimethyl ether at operating conditions from first principle microkinetic modeling and experiments, Catal. Today. 312 (2018) 35–43, https://doi.org/10.1016/j.cattod.2018.02.042.
[99] J.R. Di Iorio, A.J. Hoffman, C.T. Nimlos, S. Nystrom, D. Hibbitts, R. Gounder, Mechanistic origins of the high-pressure inhibition of methanol dehydration rates in small-pore acidic zeolites, J. Catal. 380 (2019) 161–177, https://doi.org/10.1016/j.jcat.2019.10.012.
[100] T.V.W. Janssens, S. Svelle, U. Olsbye, Kinetic modeling of deactivation profiles in the methanol-to-hydrocarbons (MTH) reaction: a combined autocatalytic-hydrocarbon pool approach, J. Catal. 308 (2013) 122–130, https://doi.org/10.1016/j.jcat.2013.05.035.
[101] P. Pérez-Uriarte, A. Ateka, A.G. Gayubo, T. Cordero-Lanzac, A.T. Aguayo, J. Bilbao, Deactivation kinetics for the conversion of dimethyl ether to olefins over a HZSM-5 zeolite catalyst, Chem. Eng. J. 311 (2017) 367–377, https://doi.org/10.1016/j.cej.2016.11.104.